Clim Dyn (2009) 32:989–1001
DOI 10.1007/s00382-008-0420-8

Predictable patterns of the Asian and Indo-Pacific summer precipitation in the NCEP CFS

Jianyin Liang · Song Yang · Zeng-Zhen Hu · Bohua Huang · Arun Kumar · Zuqiang Zhang

Received: 23 November 2007 / Accepted: 7 May 2008 / Published online: 27 May 2008

Abstract The predictable patterns of the Asian and Indo-Pacific summer precipitation in the NCEP climate forecast system (CFS) are depicted by applying a maximized signal-to-noise empirical orthogonal function analysis. The CFS captures the two most dominant modes of observed climate patterns. The first most dominant mode is characterized by the climate features of the onset years of El Niño-Southern Oscillation (ENSO), with strong precipitation signals over the tropical eastern Indian and western Pacific oceans, Southeast Asia, and tropical Asian monsoon regions including the Bay of Bengal and the South China Sea. The second most dominant mode is characterized by the climate features of the decay years of ENSO, with weakening signals over the western-central Pacific and strengthening signals over the Indian Ocean. The CFS is capable of predicting the most dominant modes several months in advance. It is also highly skillful in capturing the air–sea interaction processes associated with the precipitation features, as demonstrated in sea surface temperature and wind patterns.

Keywords Asian monsoon · Predictable patterns · NCEP climate forecast system

J. Liang
CMA Institute of Tropical and Marine Meteorology, Guangzhou, Guangdong, China

S. Yang (✉) · A. Kumar
NOAA/NWS/NCEP Climate Prediction Center, 5200 Auth Road, Room 605, Camp Springs, MD 20746, USA
e-mail: song.yang@noaa.gov

Z.-Z. Hu
Center for Ocean-Land-Atmosphere Studies, Calverton, MD, USA

B. Huang
Department of Climate Dynamics, George Mason University, Fairfax, VA, USA

Z. Zhang
CMA National Climate Center, Beijing, China

1 Introduction

The NCEP climate forecast system (CFS) provides operational seasonal prediction of the world's climate including the monsoon climate of the Asian and Indo-Pacific regions (Saha et al. 2006). In many Asian countries, CFS products are now considered important source of information for regional climate predictions (e.g. FOCRAII 2006). However, in spite of the limited information about the sub-seasonal features (Yang et al. 2008a) and seasonal-interannual variability and prediction (Wang et al. 2008; Yang et al. 2008b) of the Asian summer monsoon in the model, how competently the CFS performs in simulating and predicting the Asian–Australian and Indo-Pacific monsoon climate and its variability has not been fully documented.

The Asian–Australian monsoon is an important climate system and its variability is closely linked to many weather and climate signals both inside and outside the monsoon regions. Because of its enormous scientific and societal impacts, monsoons have a long history of academic research and operational predictions. While early studies mainly focused on the monsoon phenomenon over India (Normand 1953; Krishnamurti 1985; Shukla 1987), interest in monsoon study has been extended rapidly to a much broader region covering the entire tropical Asia and the surrounding oceans during the recent decades (Lau and Li 1984; Tao and Chen 1987; Webster and Yang 1992; and see Chang and Krishnamurti (1987) and Wang (2006) for reviews).

In this paper, we address several issues about the monsoon climate over Asia and the tropical Indo-Pacific Oceans in the CFS. We depict the predictable patterns of monsoon in CFS and assess the authenticity of the model results against observations. We also analyze the model's dynamical processes to identify the factors impacting these predictable patterns. Furthermore, we reveal the lead time for the dominant features of monsoon predicted by the model. The summer monsoon season (June–July–August; JJA) and the monsoon phenomena over both the Asian lands and the nearby waters of the Indian Ocean (IO) and western Pacific are the focus of this study.

In Sect. 2, we describe the model and data and discuss the analysis method briefly. In Sect. 3, we discuss the seasonal means of observed and model precipitation, the most predictable patterns of monsoon precipitation, and the associated physical processes. A summary of the results obtained is provided in Sect. 4.

2 Model, data, and analysis method

The NCEP CFS, whose results are analyzed in this study, is a fully coupled operational dynamical seasonal prediction system (Saha et al. 2006). The atmospheric component is the NCEP Atmospheric Global Forecast System (Moorthi et al. 2001), except for a coarser horizontal resolution with a spectral triangular truncation of 62 waves in the horizontal and 64 sigma layers in the vertical. The oceanic component is the GFDL Modular Ocean Mode V3.0 (Pacanowski and Griffies 1998). The atmospheric and oceanic components are coupled without flux adjustment, and the two components exchange time-averaged quantities once a day.

We analyze the results from the CFS retrospective predictions (or hindcasts) which cover all 12 calendar months from 1981 to 2004. These experiments, each of which is a 9-month integration, are an ensemble of 15 members starting from perturbed real-time oceanic–atmospheric initial conditions. The observed data sets used for model verification include the Climate Prediction Center Merged Analysis of Precipitation (Xie and Arkin 1996), 850-mb winds from the NCEP/DOE global reanalysis II (Kanamitsu et al. 2002), and the NOAA optimally-interpolated sea surface temperature (SST) analysis (Reynolds et al. 2002).

The main analysis tool applied in this study is a maximum signal-to-noise empirical orthogonal function (MSN EOF) method developed by Allen and Smith (1997). As in Venzke et al. (1999), Sutton et al. (2000), Huang (2004), and Hu and Huang (2007), this tool is applied to derive the patterns that optimize the signal-to-noise ratio, i.e., the leading modes are the ones that maximize the ratios of the variances of ensemble mean (the signal) to the deviations among ensemble members (the noise). Given that, in a moderate ensemble size of 15 members, the ensemble mean contains both a common evolution of all ensemble means (presumed to be the signal) and a residual random part related to the unpredictable differences among the ensemble members (internal noise), the MSN technique minimizes the effects of noise. Like a conventional EOF mode, a MSN EOF mode provides a spatial-temporal distribution. By definition, the leading MSN EOF mode represents the most predictable pattern in a hindcast system. A larger variance of this mode in the ensemble mean indicates relatively higher predictability. We apply this analysis, whose details can be found in the appendix, to document the predictable signals in precipitation over 30°S–50°N, 40°–180°E. However, additional analysis with different spatial domains (e.g. 0°–35°N, 60°–100°E) retains the major features of the patterns.

3 Results

3.1 Seasonal means of observed and model precipitation

Figure 1 shows the JJA climatological (1981–2004) means of observed and CFS ensemble-mean precipitation and 850-mb winds. For CFS, LM0 (0 month lead prediction; Fig. 1b) presents the JJA precipitation simulated using the initial conditions of 9–13, 19–23, and 30–31 May and 1–3 June. Correspondingly, LM3 (three lead months; Fig. 1c) and LM6 (Fig. 1d) present the JJA precipitation predictions using the initial conditions 3 months and 6 months, respectively, before those used in LM0.

As discussed in many previous studies (e.g. Yang and Lau 2006), the observed patterns include monsoon precipitation with large centers over western India, northern Bay of Bengal (BOB), Indo-China peninsula, South China Sea (SCS), and east of the Philippines. The patterns also include the well-known features of the southwesterly monsoon flow over tropical Asia, the Somali jet, and the tropical western Pacific anticyclone. The CFS captures most of the above features reasonably well at 0 month lead (compare Figs. 1a, b). The model also captures the Meiyu rain band over East Asia associated with the East Asia monsoon and mid-latitude frontal systems, the double rain bands over the tropical western Pacific, and the rainfall over the equatorial southern IO. However, the CFS produces unrealistic precipitations along the southern slope of the Tibetan plateau. It overestimates the precipitation over the eastern Arabian Sea and western Indo-China peninsula,

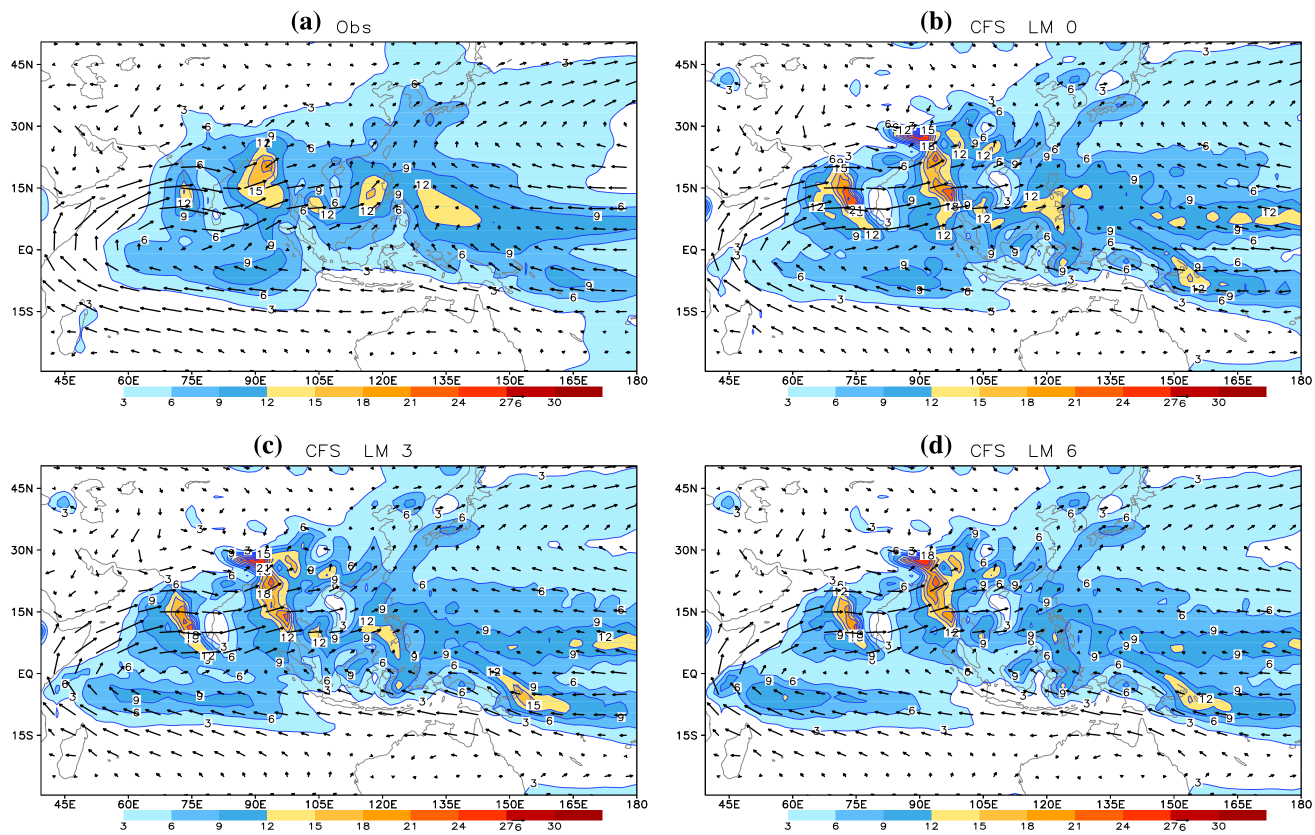

Fig. 1 JJA climatological (1981–2004) means of observed precipitation in mm per day and 850-mb winds in ms^{-1} (**a**) and CFS ensemble-mean precipitation and winds for zero lead month (**b**), three lead months (**c**) and six lead months (**d**)

and underestimates the precipitation over SCS and east of the Philippines. In addition, the mean monsoon flow and the cross-equatorial flow are relatively too weak in the model.

It can be seen from Figs. 1c–d that the patterns of LM3 and LM6 illustrate similar features to the pattern of LM0, suggesting that the CFS can correctly predict these time-mean features several months ahead. (LM6 is the longest lead month prediction available for analysis of seasonal means for this study.) The predictable features include the convection over southwestern tropical IO, the South Pacific Convergence Zone, and the East China Sea, besides the Indian monsoon precipitation. Nevertheless, from LM0 to LM6, some differences occur over the tropical IO and the far western Pacific such as the convection near the Philippines.

Figure 2 presents the standard deviations of precipitation to measure the interannual variability of the observed and CFS summer monsoon precipitation. In observations (Fig. 2a), the monsoon precipitation varies most forcefully over northern BOB, Bangladesh, and southern Indo-China peninsula. It also varies strongly over tropical southeastern IO, eastern SCS, tropical western Pacific, and the maritime continent. Relatively, small variability of monsoon precipitation appears over eastern India, western BOB and Arabian Sea, and central Indo-China peninsula along about 100°E. The CFS (Fig. 3b) captures these features reasonably well, especially those over the maritime continent, tropical southeastern IO and western Pacific, and the eastern BOB and Arabian Sea, in spite of a smaller magnitude over Bangladesh. However, the model overestimates the precipitation variability over tropical southwestern IO and Indonesia but underestimates the variability over East Asia and western North Pacific in the subtropics.

3.2 Most predictive patterns

We now depict the predictable patterns in CFS, which is capable of simulating the major climatological features of monsoon variability over Asia and the Indo-Pacific oceans, as revealed by the MSN EOF analysis. We discuss the first two most predictable modes, since only these two modes exceed the significance at 95% confidence level (*F* test). Figure 3 shows the most predictable patterns (the first mode) of precipitation and the principal component (PC) for different lead months. As in the convectional EOF analysis, the multiplication of eigenvector and PC yields values in the unit of precipitation (mm per day). The most

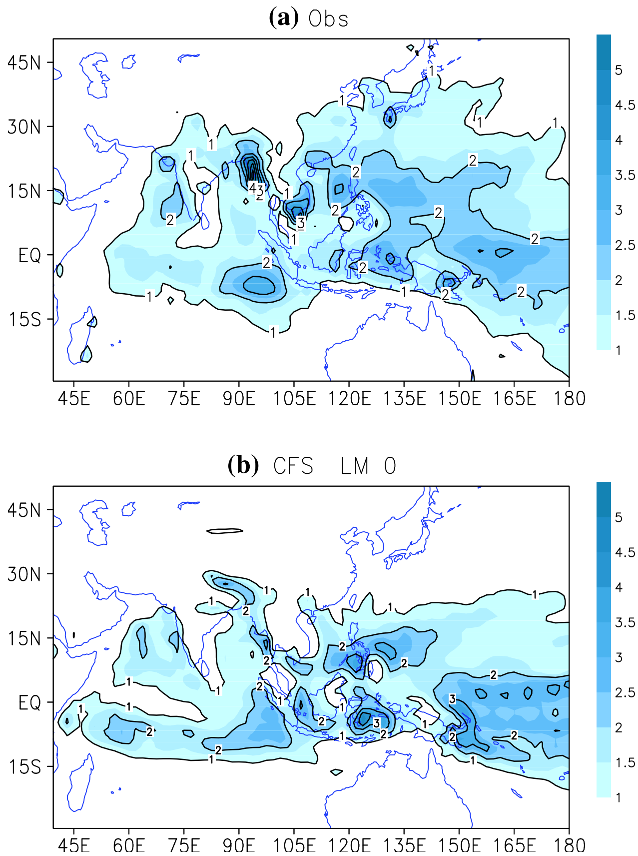

Fig. 2 Standard deviations of JJA precipitation for CMAP observation (**a**) and CFS zero lead month (**b**). Units: mm per day

striking features of Fig. 3a are the negative values (decrease in precipitation when PC is positive; and vice versa) over the equatorial central-eastern IO and Indonesia and the positive values over the equatorial western Pacific and the regions from eastern BOB to the Philippines. The figure also presents negative values over the tropical southwestern Pacific and a latitudinal band around 22°N, and positive values over the tropical western IO. Overall, the values outside 15°S–30°N are relatively small.

Figure 3b indicates that the peaks of ensemble mean PC (measured by the thick black curve) appear in the JJAs of 1982, 1987, 1991, 1993, and 1997 and the valleys in 1984–1985, 1988–1989, and 1999. Thus, the positive (negative) values in Fig. 3a measure increases (decreases) in precipitation during the summers of El Niño onset or decreases (increases) in precipitation during La Niña development. In particular, the simultaneous correlation between the PC of ensemble mean and the Nino-3.4 SST of El Niño onset years is 0.89 for LM0, 0.67 for LM3, and 0.41 for LM6, all significant at the 95% confidence level (0.41) of t test. (According to the classification of NOAA Climate Prediction Center (http://www.cpc.noaa.gov), warm ENSO event occurred in 1982–1983, 1986–1988, 1991–1992,1993, 1994–1995,1997–1998, and 2002–2003 and cold events in 1984–1985, 1988–1989, 1995–1996, and 1998–2001.) These features are also similar to the first-mode pattern of singular value decomposition analysis shown by Lau and Wu (2001). The above-depicted features are robust, as shown by the significant correlation ($R1 = 0.92$) between the PCs of ensemble mean and various members (thin dashed curves), implying that the predictions of the precipitation anomalies shown in Fig. 3a from different initial conditions are largely convergent. ($R1$ is the average value of 15 correlations between the PC of ensemble mean and the 15 PCs of ensemble members.)

Since the MSN EOF pattern is derived solely from predictions, it only represents the model preference. If a predictive model has physical deficiencies and consistently provides wrong predictions, its most predictive pattern should not be significantly correlated with observations. To determine how skillfully this highly predictable model pattern forecasts the observations, we also compute the corresponding "PC" for observations (thick dashed curve in Fig. 3b) by projecting the observed precipitation anomalies upon the spatial pattern of the first MSN EOF mode of CFS precipitation and calculate the correlation (R) between this observed "PC" and the PC of the MSN EOF (thick black curve). The correlation coefficient of 0.82 significantly exceeds the 99% confidence level, indicating that the hindcast interannual precipitation variation associated with this most predictable pattern shown in Fig. 3a is highly coherent with a portion of the observed anomalous rainfall variations. Since the PC of the MSN EOF also has comparable amplitude to its observed counterpart, it predicts the variance of the observed variations reasonably well. In other words, the model signals depicted by this MSN EOF mode largely predict the observed anomalies and R is a quantitative measure of the skill.

Figure 3 also shows that the difference between the modeled and observed patterns and the spread among various ensemble members become larger with longer leads. However, the most predictable precipitation pattern can still be detected with confidence at least 6 months in advance. This can be seen from the similarity of spatial pattern between LM3 (Fig. 3c) and LM0 (Fig. 3a), with a pattern correlation coefficient of 0.89, and between LM6 (Fig. 3e) and LM0, with a pattern correlation coefficient of 0.87. The LM3 and LM6 patterns also have a significant correlation with the observed, with $R = 0.66$ for LM3 and $R = 0.58$ for LM6. The robustness of the feature can also be seen from consistent performance among the ensemble members (on average, $R1 = 0.87$ for LM3 and $R1 = 0.86$ for LM6). Furthermore, the variances for different leads (5.23, 3.21, and 2.79) are larger than the threshold value of 1.72 of the 95% significance level (F test), suggesting that the patterns shown in Fig. 3 are statistically significant (see

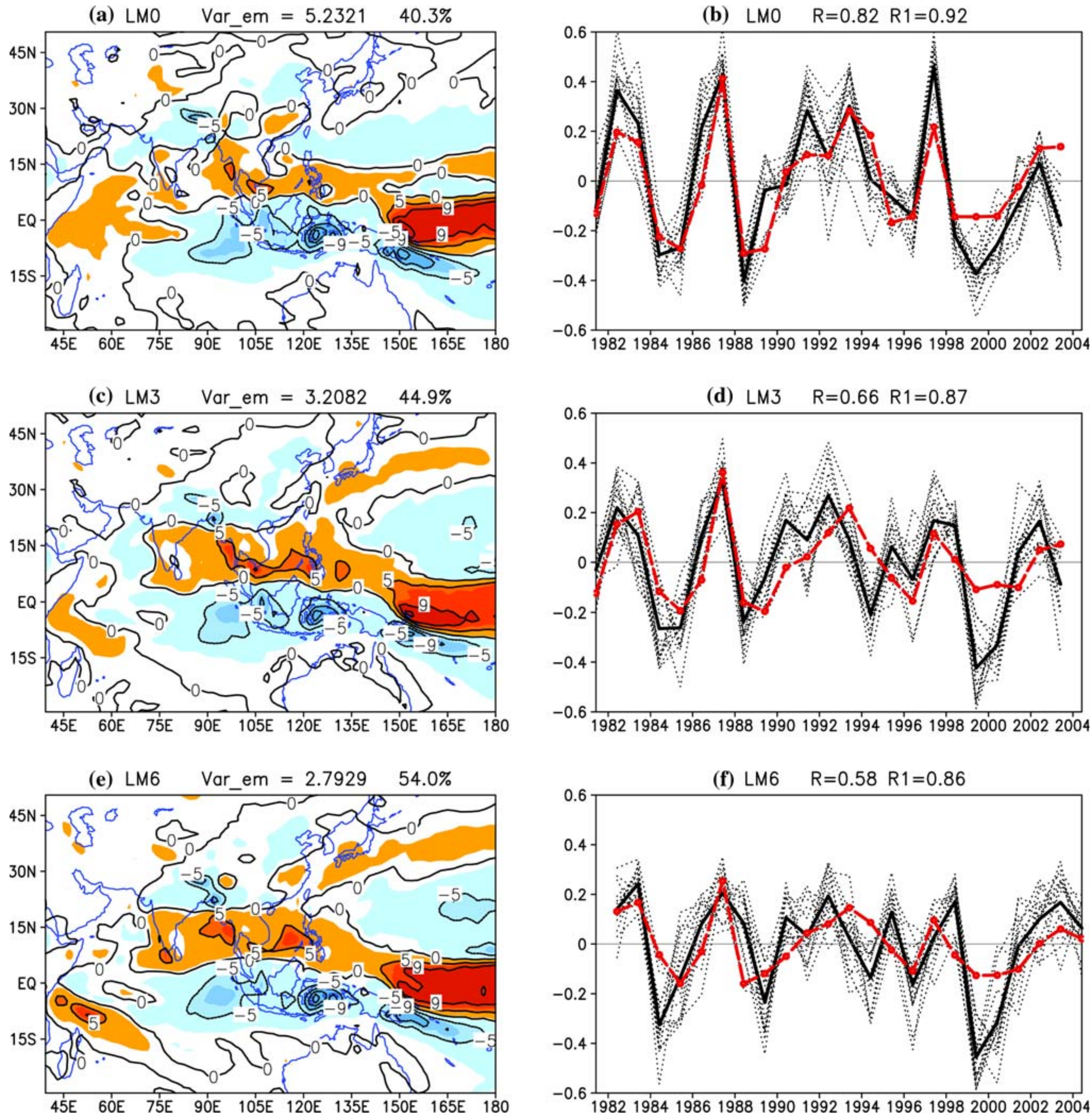

Fig. 3 First MSN EOF mode of CFS precipitation (mm per day) for lead months of 0, 3, and 6. In the right panels, the *thick solid* and *thin dashed lines* are the PCs of ensemble means and individual members, respectively. The *thick dashed lines* represent the PCs that are computed by projecting the observed precipitation upon the pattern of first mode of the CFS precipitation. *R* measures the correlation between the observation and the ensemble mean, and *R*1 measures the mean correlation among the ensemble members

Venzke et al. 1999). (The values of Var_em shown in the figure are the variances of ensemble means associated with the specified MSN EOF mode. They are calculated from the ensemble mean data projected onto the normalized first optimal filter patterns, following Vanzke et al.) The high skill for extended long-range predictions demonstrates the advantage of the MSN EOF method, which optimizes the signal-to-noise ratio by suppressing the effect of noise among the ensemble members.

The MSN EOF analysis is different from the conventional EOF analysis of the ensemble means partially because it (the former) optimizes the modes of large ratio of signal to noise and thus uses more information from ensemble members, although the two tend to yield the same patterns when the number of ensembles is infinite. It is thus interesting to compare the two analyses to better understand the noise-suppressed MSN EOF patterns and to assess the adequateness of the ensemble size. Figure 4 shows the first mode of conventional EOF for both observed precipitation and CFS precipitation (LM0, LM3, and LM6), as well as their associated PCs (right column). In general, the CFS patterns of various leads are similar to the observed pattern despite that stronger-than-observed signals appear over southern India and over southern Philippines and nearby waters in the model. Comparison between Figs. 3 and 4 also indicates a large similarity between the two analyses in corresponding leads. This implies that the number of ensemble members of CFS is adequate for predicting the major features of the most predictable mode of precipitation, at least over the western Pacific. However, differences also exist between Figs. 3 and 4, especially over tropical western IO and the subtropics (e.g. in LM0). These differences may diminish when the number of ensemble members increases. Larger difference between the two techniques occurs in the PCs. While the correlation between the MSN PC of LM0 ensemble mean and the Nino-3.4 SST of El Niño onset years is 0.89, it decreases to 0.67 for the corresponding PC of conventional EOF analysis. This difference indicates the advantage of MSN EOF analysis, which suppresses noises of ensemble simulations, in depicting the signals associated with external forcing.

Interestingly, the differences between the MSN and conventional EOFs shown in Figs. 3 and 4 diminish from short lead to longer leads. One potential explanation is that the signal-to-noise ratio may not always decay at the short leads of the hindcasts, although it will decay as the lead time increases due to the diminution of signals. As seen in Figs. 3 and 4, the percentages of total variance explained by both the MSN EOF mode and the conventional EOF mode increase monotonically with lead time. Therefore, the most dominant mode, which should mostly contain the "signals" even in the conventional EOF, counts more weight as the forecasts progress, implying that, relatively to signals, the noise level is also reducing during the hindcast. As a result, the signal-to-noise ratio may be smaller at short leads where the MSN EOF becomes more effective. The factors that possibly contribute to the high noise in the first lead month include the initial shock of the coupled system due to the imbalance between the oceanic and atmospheric initial states, which usually takes time to damp out (e.g. Chen et al. 1997; Schneider et al. 1999, 2003). Another potential explanation relates the noise levels at different lead times to the predictions initiated in different calendar months. It is conceivable that the level of both atmospheric internal variability and model error growth is seasonally dependent (e.g. Hu and Huang 2007). Its accumulative effect in the target month (e.g. June) may also be different.

For the second most predictable mode revealed by MSN EOF analysis (Fig. 5), the most noticeable features are the negative values over tropical northwestern Pacific, centered over the Philippines, and the positive values over the equatorial and northern IO (Fig. 5a). The prominent peaks (valleys) of the PC (Fig. 5b) associated with the spatial pattern appear in 1983, 1992, 1995, and 1998 (1986, 1989, and 2000–2001), the summers after El Niño (La Niña) peak events. The simultaneous correlation between this PC (PC-2) of ensemble mean and the Nino-3.4 SST of El Niño decay years is 0.80 for LM0, 0.77 for LM3, and 0.59 for LM6, all significantly exceeding the 99% confidence level (0.53) of t test. Interestingly, the signals over IO are more apparent than those seen in the first mode (Fig. 3a), suggesting that the second mode captures the delayed effect of ENSO. Overall, this second most predictable pattern is significant (with a variance of 2.63) and robust ($R1 = 0.86$) and resembles the observed features ($R = 0.80$). There exist similarities between the various lead months, with a pattern correlation coefficient of 0.83 between LM0 and LM3, and 0.67 between LM0 and LM6. In lead months of LM3 and LM6 (Figs. 5d, f), the correlations between the ensemble means and observations (R), and between the ensemble members ($R1$), are also significant, suggesting that the skill of CFS predictions for the second mode is high. However, the variances especially those for LM6 and even LM3 (Figs. 5c, e) are small. This feature suggests a relationship between signals and the ratio of signal to noise. That is, the signals of the second mode of MSN EOF optimizing the ratio of signal to noise are predictable. However, the amplitudes of these signals are small, as shown by the small variances.

Figure 6 shows the second mode of conventional EOF for observed precipitation and CFS precipitation (LM0, LM3, and LM6) and the associated PCs. As for the first mode, there is a general similarity between the observed and CFS patterns. In particular, comparison between Fig. 6a (observed) and Fig. 6c (CFS LM0) reveals many similar features over Asia and the Indo-Pacific oceans although the model yields overly strong signal over the equatorial western Pacific. Despite that there is a large similarity between the MSN EOF and the conventional EOF for the second mode, differences can also be clearly seen between Figs. 5 and 6, especially over Southeast Asia and the tropical eastern IO and western Pacific sector. Over these regions, numerical models often face difficulties in simulating the climate realistically for various reasons. The noise-suppressing MSN EOF seems superior to the conventional EOF analysis in capturing the climate signals related to external forcing. In fact, for the second mode of LM0, the correlation between the PC and the Nino-3.4 SST of the decay years of El Niño is 0.46 in the conventional EOF analysis but increases to 0.80 in the MSN EOF analysis.

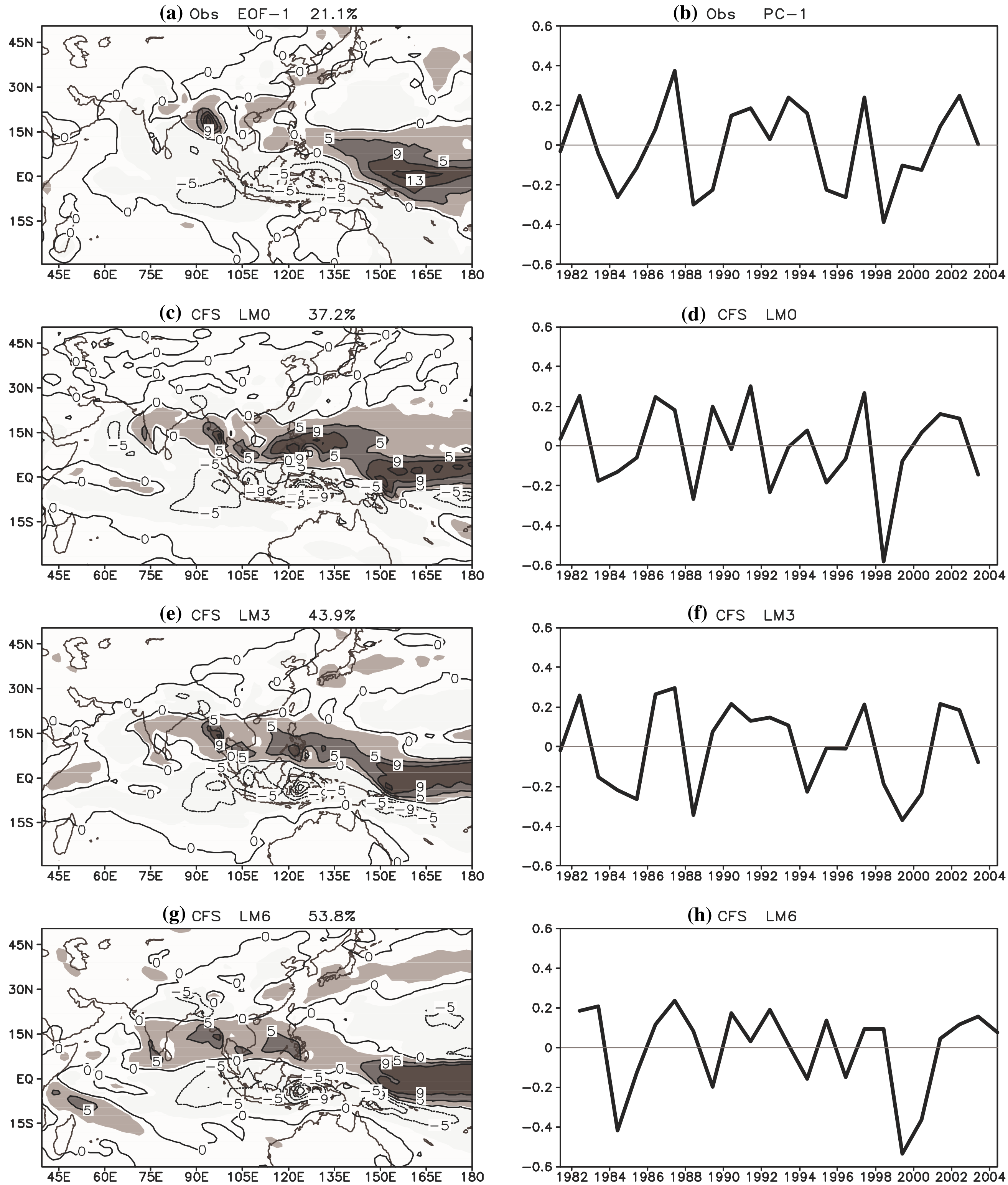

Fig. 4 First conventional EOF mode and PCs of JJA observed precipitation (**a**, **b**) and CFS precipitation for lead months of 0, 3, and 6 (**c**–**h**)

To assess whether the PCs obtained by projecting the observed precipitation upon the patterns of leading modes of CFS precipitation are affected by any possible systematic bias of the model, we further examine the relationships between the leading CFS modes that are mainly analyzed in this study and the observed

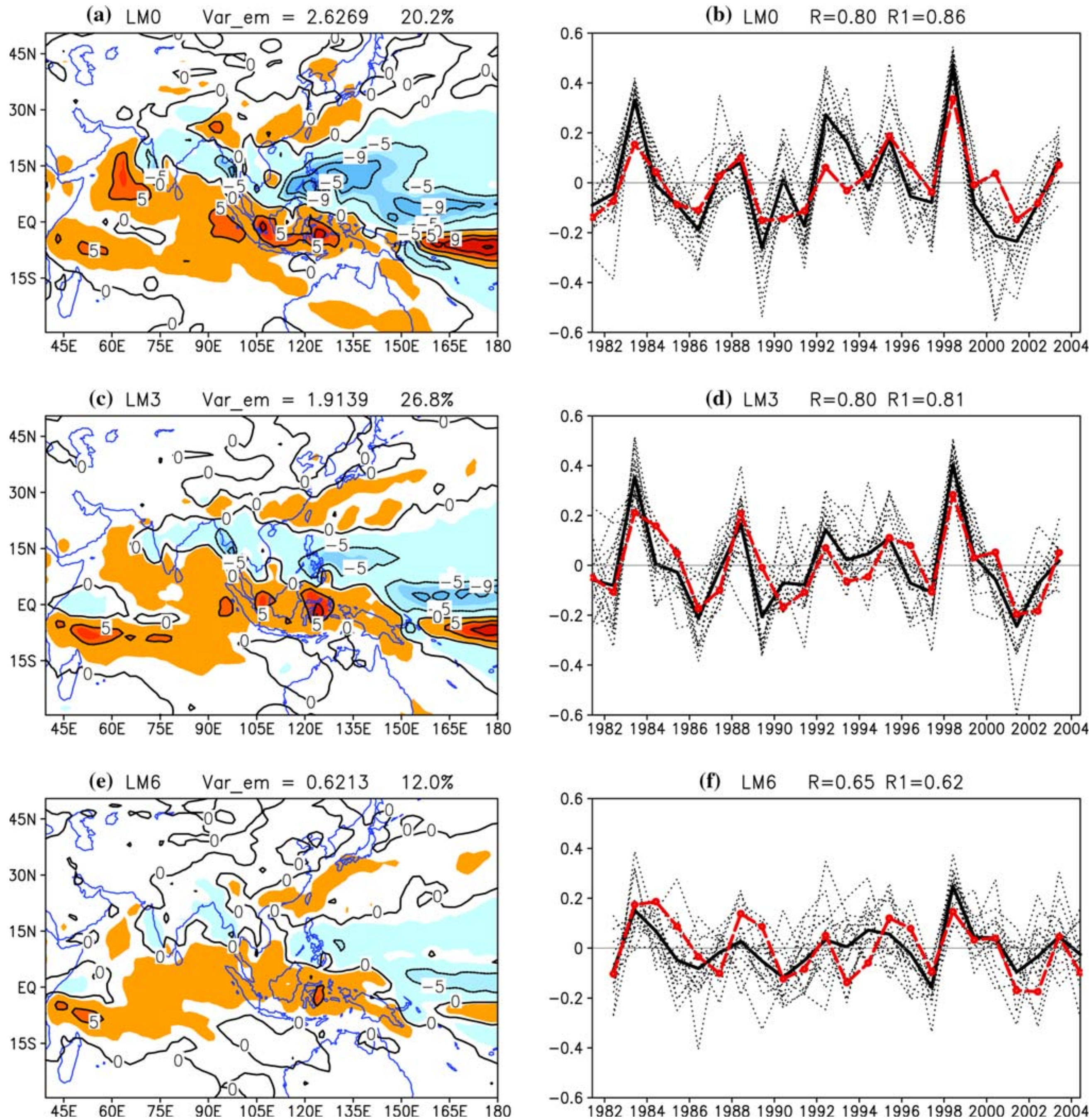

Fig. 5 Same as Fig. 3 but for the second mode

precipitation pattern. Figure 7a–c show that the most predictable mode of CFS is associated with the signals of observed precipitation mainly over Southeast Asia, the western Pacific, and the tropical eastern IO (in LM0). These signals, also appearing in Fig. 3, become weaker in longer lead months. The major observed feature associated with the second most predictable mode of CFS (Fig. 7d–f) is the opposite-sign relationship in precipitation variability between the tropical IO and subtropical North Pacific. This feature has also been seen from Fig. 5. For this mode, the correlation does not decrease with the increase in lead months, indicating an overestimate of the delayed impact of ENSO by the CFS as discussed previously.

3.3 Associated physical processes

We now analyze the patterns of SST and 850-mb winds associated with the first two most predictable modes of

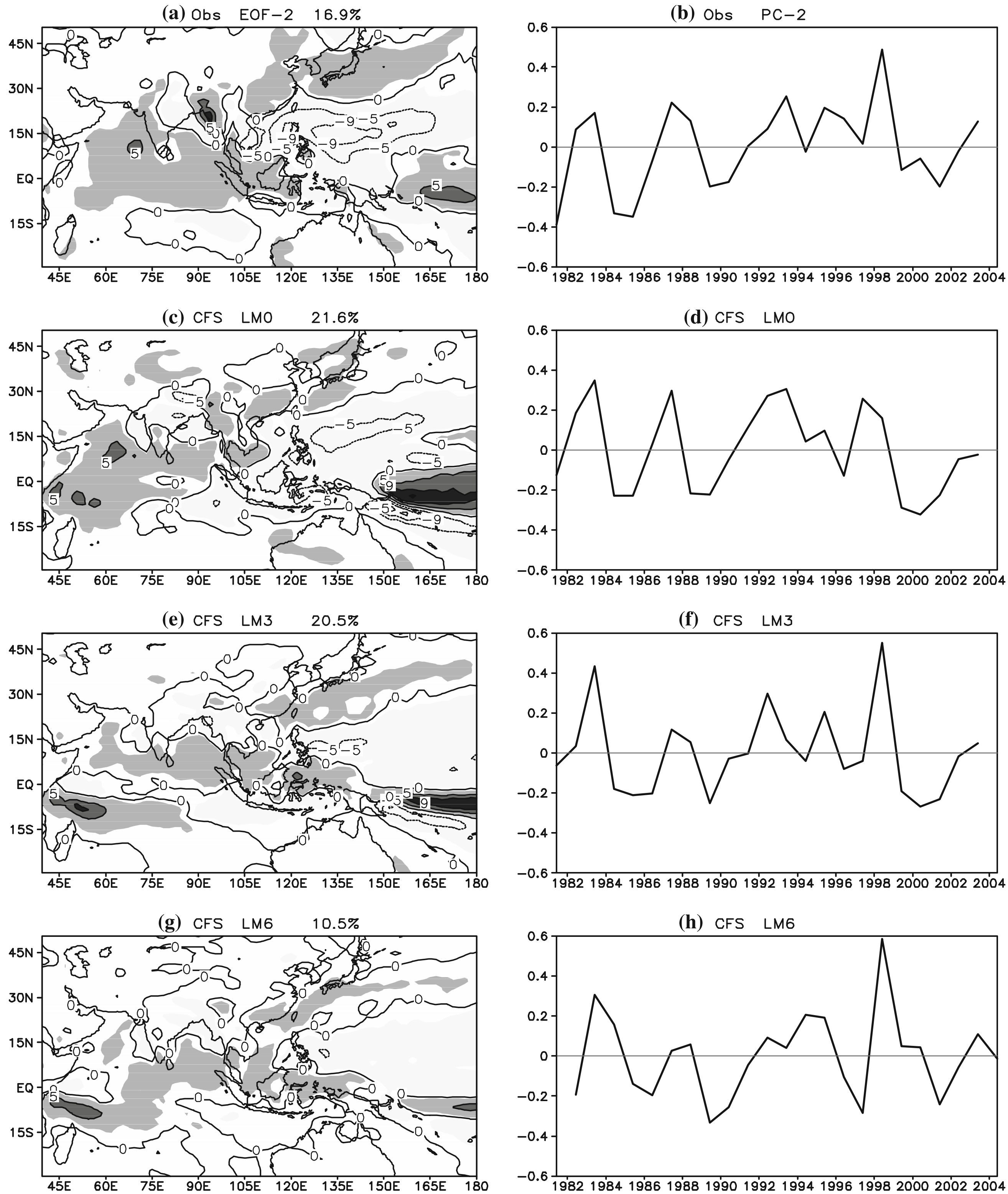

Fig. 6 Same as Fig. 4 but for the second mode

precipitation. Figure 8 shows the patterns of correlation of SST with precipitation PCs and regression of 850-mb winds against these PCs for both CFS ensemble mean of LM0 (the solid black curves in Figs. 3 and 5) and observations (the thick dashed curves). In the model (Fig. 8a), the positive values of the first PC of precipitation are

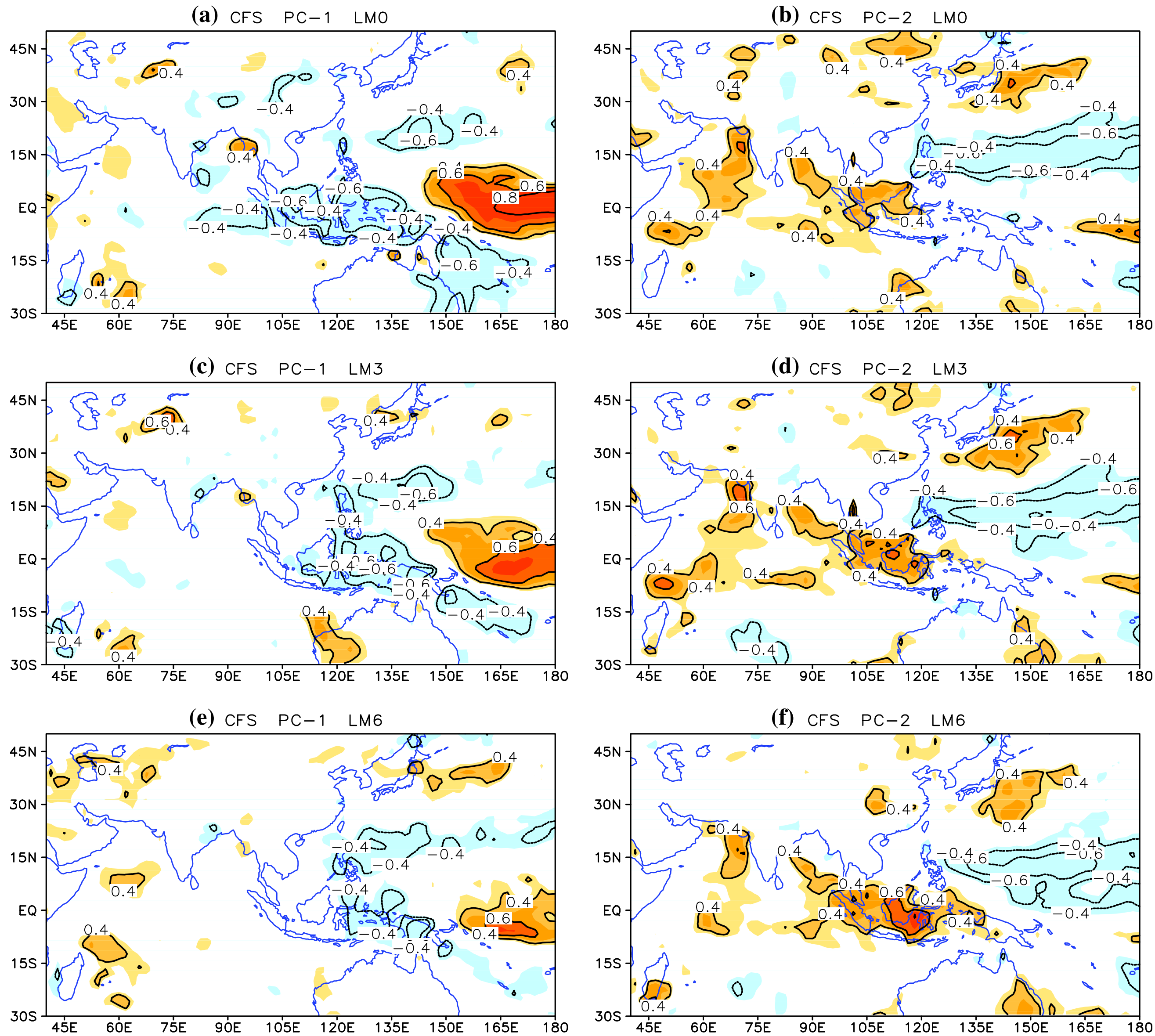

Fig. 7 JJA patterns of one-point correlation between grid-point CMAP precipitation and CFS ensemble MSN PCs of first mode (**a**–**c**) and second mode (**d**–**f**). Computations are made for lead months of 0, 3, and 6 for the CFS PCs. Significant values exceeding the 95% confidence level (*t* test) are shaded

clearly linked to warming in the equatorial central Pacific and western IO, and cooling in equatorial western Pacific, subtropical central Pacific, and tropical southeastern IO. These characteristics are similar to the features usually observed during the El Niño years (Fig. 8b; also see above discussion for Fig. 3b), except that the signals in CFS are too strong especially over the subtropical northern Pacific. In both model and observations, the SST features are associated with the weakening of easterly trade winds over the tropical Pacific and the weakening of westerly monsoon flow over the tropical IO (especially in the model). However, over BOB and SCS, the monsoon flow intensifies consistently with the increase in precipitation shown in Fig. 3. Thus, in both CFS and observations, the changes in precipitation, SST, and winds are dynamically consistent. That is, the CFS is highly skillful in capturing the air–sea interaction processes associated with the precipitation anomaly patterns. Nevertheless, as in SST, apparent difference between the modeled and observed winds emerges over the northwestern Pacific.

Two distinct features can be seen from the second mode (Figs. 8c, d). From the IO through tropical Asia to the western Pacific, both the observed and modeled westerly monsoon flows weaken clearly after the peak of El Niño (see Fig. 5b), consistent with the observational studies of Webster and Yang (1992) and Lau and Yang (1997). The weak monsoon flows are associated with warming in IO and SCS and linked to less precipitation from the Indian peninsula to the Indo-China peninsula and SCS. In both observation and model, the features over IO and SCS are more significant than those appear in the first mode (Figs. 8a, b), although the model overestimates the observed signals. The features shown in the second mode reflect the delayed effect of ENSO on IO and are consistent with the results of previous studies (Lanzante 1996; Klein 1999; Kawamura et al. 2001; Yoo et al. 2006; Yang et al. 2007).

The other important feature of the SST and atmospheric circulation patterns associated with the second most predictable pattern of CFS is the anticyclonic pattern over the tropical northwestern Pacific. As described in Wang et al. (2000) and Wang and Zhang (2002), this anticyclonic pattern, a product of air–sea interaction associated with the evolution of ENSO, plays a critical role in conveying the impact of ENSO on the climate of Southeast Asia. Clearly, the atmospheric circulation pattern leads to less precipitation over the western Pacific (see Fig. 5). In addition, the western edge of the anticyclonic pattern brings more water vapor to eastern China especially south of the Yangtze River and increases the local precipitation, a feature appearing in both observation and CFS. The features discussed above are consistent with the results of Lau et al. (2004), who have discussed the maintenance and evolution of the anticyclonic pattern and the important role of this anticyclone in linking ENSO to Southeast-East Asian climate in the GFDL general circulation model. Moreover, according to Wang et al. (2003), the anomalous anticyclone originates near the northern Philippines in the fall season of El Niño years, and then develops in winter and persists through the subsequent spring and summer. The long persistence of this anticyclonic pattern may partly account for the relatively high ensemble mean predictability with long leads.

The patterns of other lead months (figures not shown) are similar to those shown in Fig. 8 in many ways. Increase in precipitation shown in Figs. 3 and 5 is associated with cyclonic pattern or convergence of 850-mb winds, and decrease in precipitation is linked to anticyclonic pattern or divergence of the winds. The persistence of the features shown in Fig. 8 for LM0 can also be seen apparently from LM0 to LM3 and LM6.

4 Summary

The NCEP CFS is highly skillful in simulating and predicting the summer precipitation over tropical Asia and the Indo-Pacific Oceans and in capturing the air–sea

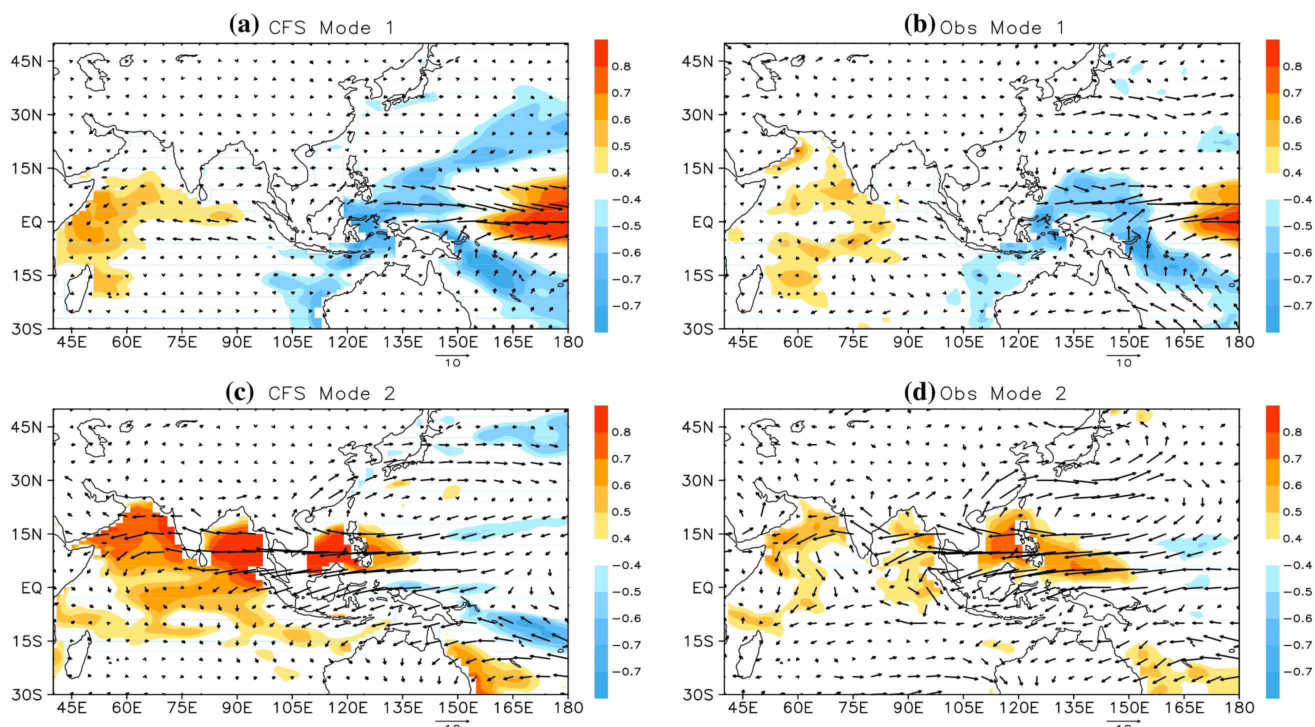

Fig. 8 **a** Correlation between grid-point SST and first principal component of LM0 ensemble-mean precipitation (shadings) and regression of 850-mb winds against the same principal component (vectors; ms^{-1}). All fields are from CFS. **b** Same as for **a** but for observations. **c**, **d** Same as **a** and **b** but for the second principal component

interaction processes associated with the patterns of precipitation anomalies as demonstrated in the variability and predictability of SST and winds. The predictable patterns revealed by applying a MSN EOF analysis largely resemble the observed climate patterns. In particular, the most predictable patterns of model precipitation are the patterns appeared in the onset years of ENSO. In these patterns, the most predictable features include the decrease in precipitation over the tropical eastern Indian Ocean and far western Pacific including Indonesia and the increase in precipitation over the tropical central Pacific and western Indian Ocean and from Indochina to the Philippines during El Niño years. The second most predictable patterns bear a resemblance to the climate patterns of the decay years of ENSO. Apparent in this mode are the decrease in precipitation over tropical northwestern Pacific, the Philippines, South China Sea, and Bay of Bengal, and the increase in precipitation over western Indonesia, southern India, and the Indian Ocean including the Arabia Sea. The weakening signals over the western Pacific and strengthening signals over the Indian Ocean are also apparent in the second mode.

Overall, the CFS is capable of predicting the most dominant modes especially the features associated with ENSO development several months in advance. However, the signals of model SST and precipitation over the western Pacific are too far westward compared to the observed, causing a too strong impact of ENSO on the monsoon.

Acknowledgments Jianyin Liang and Zuqiang Zhang, partially supported by the U.S. National Oceanic and Atmospheric Administration and the China Meteorological Administration bilateral program on climate and monsoons, thanks to NOAA's Climate Prediction Center (CPC) for hosting their visits while this study was conducted. Drs. Wanqiu Wang and Qin Zhang of CPC provided constructive comments on an earlier version of the manuscript. Zeng-Zhen Hu and Bohua Huang were supported by NOAA grant NA04OAR4310115.

Appendix

Empirical orthogonal function analysis with maximized signal-to-noise ratio

The empirical orthogonal function analysis with maximized signal-to-noise ratio (MSN EOF) applied in this study follows the exposition in Venzke et al. (1999). A description of its application has also been given in Huang (2004). The procedure is briefly outlined here simply for the convenience of reference.

In general, an ensemble mean of a CFS hindcast for a given lead month can be decomposed into the predictable and unpredictable components (i.e., $\mathbf{X_M} = \mathbf{X_P} + \mathbf{X_R}$)[1]. $\mathbf{X_P}$ depends on the common "signals" contained in all initial conditions of an ensemble and evolves consistently among its members. On the other hand, although the random internal "noises" within individual members tend to cancel each other, its residual in the ensemble mean, $\mathbf{X_R}$, is not negligible if the ensemble size is moderate, as in the case of current climate hindcast. Given a time sequence of a variable formed by multi-year hindcast with a certain lead month, we desire to find the dominant EOF pattern of $\mathbf{X_P}$, in spite of the presence of $\mathbf{X_R}$. This pattern can be defined as the most predictable pattern of the forecast system.

Assuming that $\mathbf{X_P}$ and $\mathbf{X_R}$ are temporally uncorrelated with each other, the covariance matrix ($\mathbf{C_M}$) of $\mathbf{X_M}$ can be written as the sum of the signal and residual noise covariance matrices, i.e., $\mathbf{C_M} = \mathbf{C_P} + \mathbf{C_R}$. Based on the discussion above, $\mathbf{C_R}$ is inversely related to ensemble size. In our case, $\mathbf{C_R}$ is 1/15 of the average noise covariance matrix ($\mathbf{C_N}$) from the 15 ensemble members. To find the eigenvectors of $\mathbf{C_P}$, the key procedure is to eliminate the spatial covariance of noise. Mathematically, this is equivalent to a transformation $\mathbf{F}$ such that $\mathbf{F^T C_R F} = \mathbf{I}$, where $\mathbf{I}$ is identity matrix. This transformation is referred to as the "prewhitening" in literature because the internal variation becomes white noise in the transformed space, which guarantees that $\mathbf{F^T C_P F}$ and $\mathbf{F^T C_M F}$ have identical eigenvalues. In practice, $\mathbf{F}$ is constructed from the first K weighted EOF patterns of the within-ensemble deviations $\mathbf{X_i'} = X_i - X_M$(i.e., estimated noise), where i denotes the ith member within the ensemble. K should be large enough to form an adequate basis of projection while small enough to keep the transformed matrix $\mathbf{F^T C_M F}$ well conditioned. In our case, K is chosen as 24 for a sequence of hindcast of a given month in 24 years.

The matrix of eigenvectors ($\mathbf{E}$) of $\mathbf{F^T C_M F}$ contains a set of noise filters, which can be restored to physical space by $\hat{\mathbf{E}} = \mathbf{FE}$. The optimal filter (the 1st column vector $\hat{\mathbf{e}}$ of $\hat{\mathbf{E}}$) maximizes the ratio of the variances of the ensemble mean and within-ensemble deviations. The optimally filtered time series of $\mathbf{X_M}$ (i.e., its projection onto $\hat{\mathbf{e}}$) gives the 1st MSN principal component (PC). (In practice, one can simply first project $\mathbf{X_M}$ onto $\mathbf{F}$ to form the prewhitened data in the noise EOF space and then conduct a singular value decomposition to get both $\mathbf{E}$ and all MSN PCs simultaneously.) Projecting $\mathbf{X_M}$ onto the 1st MSN PC derives the 1st MSN EOF pattern, i.e., the most predictable pattern. The subsequent patterns can be determined accordingly.

The statistical significance of an estimated MSN EOF mode (Venzke et al. 1999) can be tested as following: Using the 1st mode as an example, if there is no true signal and a derived mode is purely due to sampling, the ratio of the variance (σ_M^2) of the time series ($\mathbf{y_M}$) by projecting

[1] The bold letters represent matrix or vectors here and in following text.

$\mathbf{X_M}$ onto $\hat{\mathbf{e}}$ and the averaged within-ensemble variance (σ_N^2) of the time series ($\mathbf{y_k}$) by projecting $\mathbf{X}'_\mathbf{k}$ onto $\hat{\mathbf{e}}$ obeys an F-distribution:

$$n\frac{\sigma_M^2}{\sigma_N^2} = n\frac{\frac{1}{m-1}\mathbf{y_M^T y_M}}{\frac{1}{(m-1)(n-1)}\sum_k \mathbf{y_k^T y_k}} \sim F_{m-1,(m-1)(n-1)} \qquad \text{(A1)}$$

Here m is the number of sampling times and n the total members within the ensemble. We will only consider those modes that pass the 95% significance level in this test.

References

Allen MR, Smith LA (1997) Optimal filtering in singular spectrum analysis. Phys Lett 234:419–428

Chang CP, Krishnamurti TN (1987) Monsoon meteorology. Oxford University Press, London

Chen D, Zebiak SE, Cane MA, Busalacchi AJ (1997) Initialization and predictability of a coupled ENSO forecast model. Mon Weather Rev 125:773–788

FOCRAII (2006) Second session of the forum on regional climate monitoring, assessment and prediction for Asia. 6–8 April 2006, Beijing, China (available at http://www.wmo.ch/web/wcp/ccl/topics/FOCRAII-summary_1_1.pdf#search = %22FOCRAII%20Summary%22)

Hu ZZ, Huang B (2007) The predictive skill and the most predictable pattern in the tropical Atlantic: the effect of ENSO. Mon Weather Rev 135:1786–1806

Huang B (2004) Remotely forced variability in the tropical Atlantic Ocean. Clim Dyn 23:133–152

Kanamitsu M, Ebisuzaki W et al (2002) NCEP-DOE AMIP-II Reanalysis (R–2). Bull Am Meteorol Soc 83:1631–1643

Kawamura R, Matsuura T, Satoshi I (2001) Role of equatorially asymmetric sea surface temperature anomalies in the Indian Ocean in the Asian summer monsoon and El Nino-Southern Oscillation coupling. J Geophys Res 106:4681–4693

Klein S (1999) Remote sea surface temperature variations during ENSO: Evidence for a tropical atmospheric bridge. J Clim 12:917–932

Krishnamurti TN (1985) Summer monsoon experiment—a review. Mon Weather Rev 113:1590–1620

Lanzante JR (1996) Lag relationships involving tropical SSTs. J Clim 9:2568–2578

Lau KM, Li MT (1984) The monsoon of East-Asia—a survey. Bull Am Meteorol Soc 65:114–125

Lau KM, Wu HT (2001) Principal modes of rainfall-SST variability of the Asian summer: a reassessment of the monsoon-ENSO relationship. J Clim 14:2880–2895

Lau KM, Yang S (1997) Climatology and interannual variability of the Southeast Asian summer monsoon. Adv Atmos Sci 14:141–162

Lau NC, Nath MJ, Wang B (2004) Simulations by a GFDL GCM of ENSO-related variability of the coupled atmosphere-ocean system in the East Asian monsoon region. East Asian Monsoon (Ed by Chang CP). World Scientific, Mainland Press, Singapore, pp 271–300

Moorthi S, Pan HL, Caplan P (2001) Changes to the 2001 NCEP operational MRF/AVN global analysis/forecast system. NWS Tech Pro Bull 484, pp 14 (available at http://www.nws.noaa.gov/om/tpb/484.htm)

Normand C (1953) Monsoon seasonal forecasting. Q J Roy Meteorol Soc 79:463–473

Pacanowski RC, Griffies SM (1998) MOM3.0 Manual. NOAA/GFDL, Princeton, 08542

Reynolds RW, Rayner NA et al (2002) An improved in situ and satellite SST analysis for climate. J Clim 15: 1609–1625

Saha S, Nadiga S, Thiaw C et al (2006) The NCEP climate forecast system. J Clim 19: 3483–3517

Schneider EK, Huang B, Zhu Z, DeWitt DG, Kinter JL, Kirtman BP, Shukla J (1999) Ocean data assimilation, initialization, and predictions of ENSO with a coupled GCM. Mon Weather Rev 127:1187–1207

Schneider EK, DeWitt DG, Rosati A, Kirtman BP, Ji L, Tribbia JJ (2003) Retrospective ENSO forecasts: sensitivity to atmospheric model and ocean resolution. Mon Weather Rev 131:3038–3060

Shukla J (1987) Interannual variability of monsoons. Monsoons (Ed by Fein JS and Stephens PL), Wiley, Inc, pp 399–463

Sutton RT, Jewson SP, Rowell DP (2000) The elements of climate variability in the tropical Atlantic region. J Clim 13:3261–3284

Tao S, Chen L (1987) A review of recent research on East Asian monsoon in China. Monsoon meteorology (Ed by Chang CP and Krishnamurti TN), Oxford University Press, London, pp 60–92

Venzke S, Allen MR et al (1999) The atmospheric response over the North Atlantic to decadal changes in sea surface temperature. J Clim 12:2562–2584

Wang B (2006) The asian monsoon. Praxis Publishing Ltd, Chichester, p 787

Wang B, Zhang Q (2002) Pacific–East Asian teleconnection Part II: how the Philippine Sea anomalous anticyclone is established during El Niño development. J Clim 15:3252–3265

Wang B, Wu R, Fu X (2000) Pacific–East Asian teleconnection: how does ENSO affect East Asian climate? J Clim 13:1517–1536

Wang B, Wu R, Li T (2003) Atmosphere-warm ocean interaction and its impacts on Asian–Australian monsoon variation. J Clim 16:1195–1211

Wang B, Lee JY, Kang IS et al (2008) How accurately do coupled climate models predict the leading modes of the Asian-Australian monsoon interannual variability? Clim Dyn 30:605–619

Webster PJ, Yang S (1992) Monsoon and ENSO: selectively interactive system. Q J Roy Meteorol Soc 118:877–926

Xie P, Arkin PA (1996) Analyses of global monthly precipitation using gauge observations, satellite estimates, and numerical model predictions. J Clim 9:840–858

Yang S, Lau KM (2006) Interannual variability of the Asian monsoon. The Asian Monsoon (Eds. Wang B, pp. 787), Praxis Publishing Ltd, Chichester, UK, pp 259–293

Yang S, Ding X, Zheng D, Yoo SH (2007) Time-frequency characteristics of the relationships between tropical Indo-Pacific SSTs. Adv Atmos Sci 24:1–17

Yang S, Wen M, Higgins RW (2008a) Sub-seasonal features of the Asian summer monsoon in the NCEP Climate Forecast System. ACTA Oceanol Sin (in press)

Yang S, Zhang Z, Kousky VE, Higgins RW, Yoo SH, Liang J, Fan Y (2008b) Simulations and seasonal prediction of the Asian summer monsoon in the NCEP Climate Forecast System. J Climate (in press)

Yoo SH, Yang S, Ho CH (2006) Variability of the Indian Ocean sea surface temperature and its impacts on Asian-Australian monsoon climate. J Geophys Res 111: D03108. doi:10.1029/2005JD006001